Factors controlling the summer *Emiliania huxleyi* bloom in the Black Sea: A modeling study

Temel Oguz [a,*], Agostino Merico [b]

[a] *Institute of Marine Sciences, Middle East Technical University, PO Box 28, Erdemli 33731, Turkey*
[b] *School of Ocean and Earth Science, Southampton Oceanography Center, Southampton, UK*

Abstract

A one-dimensional coupled physical–ecosystem model identifies factors causing blooms of the coccolithophore *Emilania huxleyi* in the Black Sea, regularly observed during the early summer periods. The model specifically applies for a more idealized ecosystem of the interior basin, away from the coastal zone. It is represented in the form of four groups of phytoplankton (diatoms, dinoflagellates, *E. huxleyi*, a small phytoplankton group), and two groups of zooplankton further accompanied by simplified nitrogen and phosphorus cycles. The simulations show that the internal trophodynamic conditions in the Black Sea support *E. huxleyi* bloom development during May–July period as a part of the seasonal phytoplankton succession. They start flourishing after the diatom and dinoflagellate blooms under nitrogen depleted and moderate light conditions. They make use of regenerated nutrients available in the surface mixed layer and grow concomitantly with picophytoplankton community in the subsurface levels.
© 2005 Elsevier B.V. All rights reserved.

1. Introduction

The classical seasonal phytoplankton dynamics in the Black Sea consists of a strong diatom and dinoflagellate-dominated spring production, followed by a weaker mixed assemblage of community development below the seasonal thermocline during summer months and a surface-intensified autumn production (Moncheva and Krastev, 1997; Mikaelyan, 1997; Eker et al., 1999; Eker-Develi and Kideys, 2003; Sorokin, 2002; Soydemir et al., 2003). This annual phytoplankton community structure is further accompanied with *E. huxleyi* population during the late spring and summer months within the shallow surface mixed layer, as documented by the in situ and sediment trap measurements (Benli, 1987; Hay and Honjo, 1989; Mankovsky et al., 1996; Uysal et al., 1998; Eker et al., 1999, Eker-Develi and Kideys, 2003), as well as remote-sensing observations (Sur et al., 1994; Cokacar et al., 2001, 2004; Cokacar, 2005).

The percent areal coccolith coverages deduced from the weekly SeaWiFS normalized water-leaving radiance data for the 1997–2002 period (Cokacar et al., 2004) indicate that coccoliths emerge typically during mid-May, reach the strongest phase with almost basinwide coverage throughout June, and finally disappear by mid-July (Fig. 1). Even though the Black Sea early summer coccolithophore blooms are weaker than their counterparts in other regions of the world oceans, nevertheless they are one of the most
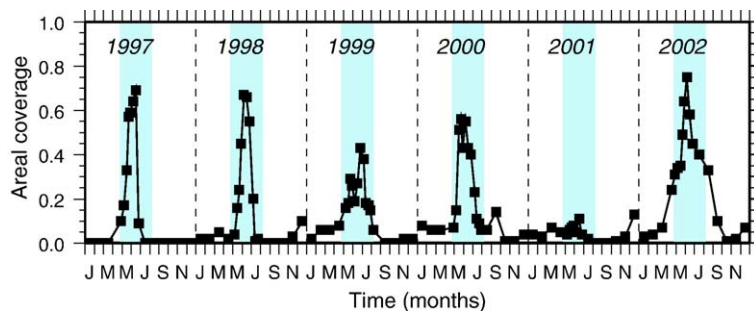
Fig. 1. Time series of areal coccolith coverage as a percentage of the total area of the basin obtained by the sum of pixels satisfying coccolithophore bloom conditions (after Cokacar et al., 2004). The gray-shaded zones represent the May–July period in which coccolithophore blooms occur in the Black Sea. This plot is based on the analysis of the weekly (8-day) and monthly, 9 km resolution normalized water leaving radiance SeaWiFS Level 3 data provided by the NASA-Distributed Active Archive Center (DAAC).

persistent and robust feature of the annual phyto-plankton structure of the Black Sea ecosystem. The SeaWiFS observations shown in Fig. 1 suggest their almost basinwide coverage in 5 years out of a total of 6 years of data comprising the 1997–2002 period. An indication of similar persistent structure of the early-summer coccolithophore blooms has also been pro-vided by the analysis of the 20 year-long (1983–2002) AVHRR time series data (Cokacar, 2005). An indirect evidence of the Black Sea *E. huxleyi* bloom developments has been given by enhanced methane-sulfonic acid (MSA) concentrations measured at two coastal stations located along the Mediterranean coast of Turkey and the island Crete (Kubilay et al., 2002). Timing of these local high MSA concentrations ap-parently coincided with the summer Black Sea *E. huxleyi* blooms, known to be major dimethyl sulfide (DMS) releaser to the atmosphere, and its transport towards the Aegean–Eastern Mediterranean Sea re-gion by persistent low level northerly winds.

In spite of their global scale impacts due to release of high rate of DMS and contribution to pCO_2 in-crease through production of $CaCO_3$ coccoliths, bloom dynamics of coccolithophores in general and of *E. huxleyi* in particular have received limited at-tention in biological models. Aknes et al. (1994) provided a simple, process-oriented model designed to interpret a set of mesocosm experiments. Tyrrell and Taylor (1996) explored factors leading to merid-ional variations of *E. huxleyi* population in the north-east Atlantic. Merico et al. (2004) investigated the causes of *E. huxleyi* blooms recently observed in the Bering Sea shelf. Iglesias-Rodriguez et al. (2002) inferred spatio-temporal characteristics of coccolitho-phore blooms in the world oceans diagnostically using SeaWiFS data.

None of the ecosystem models of differing com-plexity developed so far for the Black Sea (Lebedeva

and Shushkina, 1994; Oguz et al., 1996, 1999, 2001; Gregoire et al., 1998, 2004; Lancelot et al., 2002) has included coccolithophores as an independent group in spite of their fairly complex food web representations. The present work extends an existing intermediate-complexity ecosystem model (Oguz et al., 1999) to include coccolithophores as a part of the Black Sea phytoplankton community structure. The first objective of this study is thus to provide quantitative support for *E. huxleyi* blooms in the Black Sea as a part of the seasonal phytoplankton species succession in response to the basin's internal trophodynamic conditions. The second objective is to examine sensitivity of these blooms to various envi-ronmental factors and to identify major processes controlling their development. The present model also provides a general framework for the implemen-tation of coccolithophore dynamics in ocean carbon cycle models, whose more systematic treatment is timely and demanding.

2. Model description

2.1. General model structure

The model involves simultaneous solutions of a set of one-dimensional equations for the physical and ecosystem modules representing the areal-averaged conditions of the interior deep part (>1500 m depth) of the Black Sea, away from the shelf and topographic slope zone around the basin. The vertical domain of the model extends from the surface down to 150 m, which roughly corresponds to the lower boundary of the permanent pycnocline separating the less saline and biologically active upper layer from more dense and biologically inert, anoxic layer. The vertical structure is resolved by 50 vertical levels, which provide a grid spacing of ~3 m to accommo-

date strong vertical gradients of the physical and biogeochemical structures.

The physical model, described previously by Oguz et al. (1996, 1999), computes the yearly evolution of the flow and stratification characteristics under given climatological monthly-mean wind stress, heat and fresh water fluxes prescribed at the surface by solving two components of the horizontal momentum and temperature, salinity equations. This knowledge of the flow system is then used to compute the vertical turbulent mixing coefficient by means of the 2.5 level Mellor–Yamada turbulent closure scheme. Thus, the vertical structures of temperature and vertical diffusion coefficient used are provided to the ecosystem model prognostically at each time step by the physical model. For their model simulated annual structures, we refer to Fig. 6a, b in Oguz et al. (1999).

The ecosystem model is an extended version of the seven compartment (two phytoplankton, two zooplankton, detritus, ammonium and nitrate) model of Oguz et al. (1999). The new model includes members of the three most dominant phytoplankton taxonomic groups observed in the Black Sea comprising Bacillariophyta (diatoms, P_d), Dinophyta (dinoflagellate, P_f) and Chrysophyta (coccolithophore *E. huxleyi*, P_e). Phytoflagellates and picophytoplankton constitute the smallest members of the observed community structure. They are included as the fourth phytoplankton compartment into the model as the small size (<5 μm) phytoplankton group (P_s), hereinafter also referred to as the picophytoplankton group. The zoo-

plankton community is simply represented by microzooplankton Z_s (*<50* μm), and mesozooplankton Z_l (*>50* μm) groups. They consume different phytoplankton groups with different preferences, as specified in grazing terms.

All plankton biomass are expressed in nitrogen units; nitrogen is considered to be the most important limiting nutrient for the interior Black Sea ecosystem with respect to silicate and phosphate. The data collected from field measurements in various parts of the interior Black Sea during the 1990s indicate N:P ratio typically less than 8 (Fig. 2a). This implies preferential growth of *E. huxleyi* in the Black Sea under nitrogen limited conditions, as in the case of the Bering Sea (Tyrrell and Merico, 2004). The model, however, includes a simplified phosphorus cycle in order to explore competitiveness of *E. huxleyi* blooms under phosphorus limitation as suggested by Reigman et al. (1992), Egge and Heimdal (1994), Tyrrell and Taylor (1996). The data shown in Fig. 2b suggest relative silicate abundance with respect to nitrogen. The Si:N ratio reveals values greater than 5, which are considerably higher than the Si:N values of 1-to-3 reported in the literature for various silicate-limited ecosystems. Thus, silicate does not limit diatom growth in the Black Sea.

The simplified nitrogen and phosphorus cycles involve labile pelagic detrital nitrogen (D_n) and detrital phosphorus (D_p), as well as dissolved inorganic nitrate (N_n), ammonium (N_a), and phosphate (N_p). Attached and detached coccolith concentrations constitute two
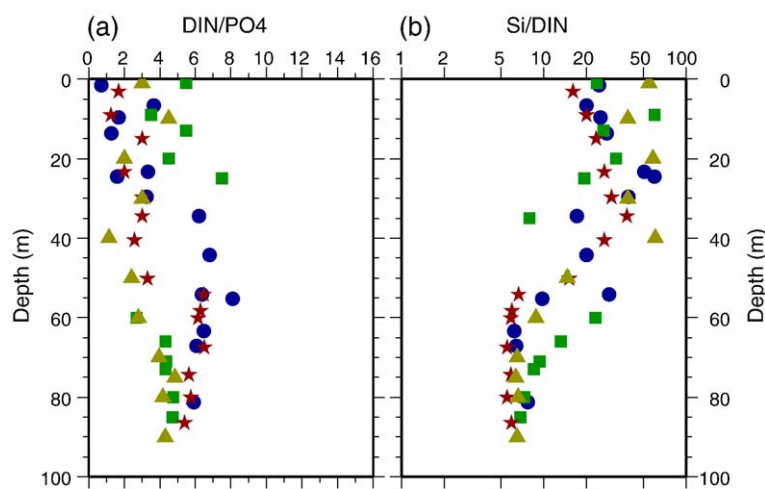

Fig. 2. Vertical profiles of (a) dissolved inorganic nitrate to phosphate (DIN/PO₄), and (b) silicate to nitrate (Si/DIN) at four stations representative of the interior basin characteristics of the Black Sea. Triangles show measurements at 42°15′ N, 29°15′ E during 18 March 1995 (western gyre); squares at 41°58′ N, 29°56′ E during 28 May 2001 (western gyre); solid circles at 42°45′ N, 36°45′ E during 03 October 1999 (central basin); stars at 42°30′ N, 37°45′ E during 22 April 1998 (eastern gyre). The profiles shown here are chosen from the R.V Bilim measurements archived at the Middle East Technical University, Institute of Marine Sciences data base (after Oguz, 2005).

additional prognostic variables. The ecosystem model thus comprises a total of 13 state variables.

Oxygen cycling and redox processes across the suboxic–anoxic interface, incorporated previously by Oguz et al. (2000), are excluded here in order to reduce the model complexity as they are not the primary concern of the *E. Huxleyi* bloom dynamics. Similarly, gelatinous carnivores and microbial loop have not been included in the present model since *E. huxleyi* are not tightly coupled with them in terms of prey–predator interactions. These features of the Black Sea ecosystem have been studied in some details by Oguz et al. (2001). The model, which is specifically applied here for the Black Sea food web configuration, should be fairly representative for other temperate basin ecosystems with some modifications. The governing equations of the model are provided in Appendix A.

2.2. Boundary conditions

Due to the presence of the suboxic and anoxic layers below the oxygenated and biologically productive surface layer, the Black Sea vertical biogeochemical structure differs from that of other oxygenated seas. The distinction comes from diminishing oxygen and nitrate concentrations immediately below the biologically active surface layer of about 50 m. The suboxic layer is characterized by low oxygen concentration of less than 10 μM and rapid decrease of nitrate concentrations from the peak values of 6–8 μM at its upper boundary at around 75 m to zero at the suboxic–anoxic boundary, which is typically located at depths around 100–125 m for the cyclonic interior basin where the present model is applied. The rapid depletion of oxygen and nitrate in this transitional layer occurs due to consumption of first oxygen and then nitrate during oxidation of detrital material before they are lost to the deep anoxic pool (Murray et al., 1995; Kuypers et al., 2003). The anoxic layer further below, therefore, does not contain any dissolved inorganic nitrate.

Sediment trap observations (e.g. Lebedeva and Vostokov, 1984; Karl and Knauer, 1991) suggest intense remineralization of organic material before reaching the anoxic layer. It has been shown that about 90% of detrital material is remineralized within approximately the upper 100 m. The remainder is lost to the deep. In reality, this loss is compensated from coastal sites. However, prescription of lateral fluxes is not a straightforward issue in one dimensional vertical models. In the present model, this difficulty is avoided by allowing complete remineralization of the settling particles within the upper layer water column by the choice of relatively low detrital settling speed of 6.0 m d^{-1} and fast remineralization rate of 0.1 d^{-1}. Because the ecological model is fully conservative (i.e. $\sum \Re(F) = 0$ in our model; see Appendix), the complete remineralization avoids dealing with specification of any nitrate-based input flux to compensate export flux of detrital material at the bottom boundary. As a result, diatom, detrital nitrogen and phosphorus equations are complemented by the absence of sinking fluxes at both the surface and bottom boundaries. Moreover, all turbulent diffusive fluxes are also set to zero at these boundaries.

2.3. Initial conditions, numerical procedure and parameters setting

The ecosystem model is initialized by an idealized vertically uniform nitrate and phosphate profiles. Nitrate and phosphate concentration are set to 4 mmol N m^{-3} and 0.25 mmol P m^{-3} within the upper 100 m layer, respectively. Further below down to the lower boundary of the model, values of zero and 0.5 mmol P m^{-3} are chosen, respectively. Other state variables are initialized with small constant values to allow positive growth and utilization. Once the model equations are integrated ahead in time, the internal dynamics (i.e. plankton productivity, nitrogen cycling, and vertical mixing) gradually establish realistic structures of all state variables, after a few years of transient adjustment. The final, equilibrium solution then develops merely on the basis of internal trophodynamic structure of the model.

The second order Leapfrog time difference and centered space difference are used to discretize the set of equations governing the physical and ecosystem models. The vertical differencing is implicit to avoid computational instabilities generated by the use of small grid spacing of 3 m. The separation of solutions associated with the Leapfrog time differencing is avoided by applying a time filter to the solutions at each time step. A time step of 10 min is used in the numerical integration of the system of equations. First, the physical model is integrated independently for five years to achieve a yearly cycle of the upper layer physical structure. Using the results of the fifth year cycle of the physical model, the ecosystem model is then integrated for another five years. The transient adjustment of the ecosystem model is completed by the end of the second year, and all solutions attain their steady-state forms within the fourth year of integration. The analysis

Table 1
Definition of parameters and their values used for phytoplankton groups

Definition	Diatom	Dinoflag.	*E. huxleyi*	Small Phyto.
Initial slope of the *PI* curve (m^2 W^{-1})	a_d=0.01	a_f=0.01	a_e=0.005	a_p=0.01
Maximum phytoplankton growth rate (d^{-1})	g_d=2.9	g_f=1.3	g_e=2.2	g_s=1.65
Q_{10} parameter for temperature limitation	Q_d=1.5	Q_f=1.5	Q_e=1.5	Q_s=1.5
Phytoplankton Mortality rate (d^{-1})	λ_d=0.06	λ_f=0.06	λ_e=0.06	λ_s=0.06
Half saturation constant for nitrate uptake (mmol N m^{-3})	K_{nd}=0.5	K_{nf}=0.23	K_{ne}=0.38	K_{ns}=0.3
Half saturation constant for ammonium uptake (mmol N m^{-3})	K_{ad}=0.2	K_{af}=0.2	K_{ae}=0.1	K_{as}=0.2
Half saturation constant for phosphate uptake (mmol P m^{-3})	K_{pd}=0.05	K_{pf}=0.05	K_{pe}=0.005	K_{ps}=0.05
Food preference coefficient of mesozooplankton	b_{ld}=0.6	b_{lf}=0.3	b_{le}=0.05	b_{ls}=0.15
Food preference coefficient of microzooplankton	b_{sd}=0.2	b_{sf}=0.0	b_{se}=0.6	b_{ss}=0.2

of the results presented in the subsequent sections is based on the fifth year of integration of the ecosystem model.

The parameter values are chosen from the published Black Sea literature, mostly from our previous models (Oguz et al., 1996, 1999, 2001), and are given in Tables 1–3. Those for coccolithophores, which were not available locally, are taken from model studies for other seas with similar pelagic ecosystem characteristics (e.g., Aknes et al., 1994; Tyrrell and Taylor, 1996; Merico et al., 2004). As suggested by Hulburt (1990), growth rate of *E. huxleyi* is greater than other small phytoplankton groups (such as flagellates), and comparable to diatoms. Thus, following the previous studies, the model specifies a maximum growth rate of 2.2 d^{-1} for *E. huxleyi*, which is in between that of 2.9 d^{-1} for diatoms and 1.65 d^{-1} for small phytoplankton group. Dinoflagellates attain the smallest maximum growth rate of 1.3 d^{-1}. We note that these maximum growth rates are subject to further reduction by Q_{10} factor at temperatures lower than 20 °C. Half-saturation constants for nitrate uptake are taken proportional to the growth rates of phytoplankton groups as in Aknes et al. (1994). This specification provides a competitive advantage to *E. huxleyi* population with respect to small phytoplankton group. Similar competitive advantage is also assigned for ammonium and phosphorus uptakes by choosing its half saturation constants as 0.1 mmol N m^{-3} and 0.005 mmol P

m^{-3}, respectively; the corresponding values for the other groups are 0.2 mmol N m^{-3} and 0.05 mmol P m^{-3}. Another distinguishing feature of *E. huxleyi* population is their relative disadvantage of growth at low light levels, and advantage at high light levels as compared to all other phytoplankton groups. This characteristic feature of *E. huxleyi* is specified in the model by assigning a relatively lower value (0.005 m^2 W^{-1}) for the initial slope of the *PI* curve with respect to the other groups (0.01 m^2 W^{-1}).

Table 3
Definition of some parameters and their values

Definition	
Light exctinction coefficient for PAR in pure water (m^{-1})	k_w=0.07
Self-shading coefficient due to phytoplankton (m^{-1} mmol N m^{-3})	k_p=0.05
Self-shading coefficient due to detritus, cocoliths (m^{-1} mmol N m^{-3})	k_c=0.05
Ammonium inhibition parameter for nitrate uptake (mmol N m^{-3})$^{-1}$	φ=3.0
Nitrification rate (d^{-1})	Ω_a=0.1
Remineralization rate for particulate nitrogen (d^{-1})	ε_n=0.1
Remineralization rate for particulate phosphate (d^{-1})	ε_p=0.1
Phosphorus to nitrogen ratio	r_{PN}=1/10
Diatom sinking rate (m d^{-1})	W_p=1.0
Detritus sinking rate (m d^{-1})	W_d=6.0
Food preference coef. of mesozooplankton on microzooplankton	b_{ls}=0.2
Food preference coefficient of mesozooplankton on detritus	b_{ldet}=0.5
Food preference coefficient of microzooplankton on detritus	b_{sdet}=1.0
Maximum calcification rate (d^{-1})	C_{max}=2.0
Carbon to Nitrogen ratio (mg C/mmol N)	r_{CN}=12*6.625
Dissolution rate of calcite of detached cocoliths (d^{-1})	θ=0.05
Minimum detachment rate of cocoliths (d^{-1})	$\Gamma_{d,min}$=0.1
Maximum detachment rate of cocoliths (d^{-1})	Γ_d=10.0
Maximum number of excess cocoliths (mg calcite C/mg org. C)	Π_{max}=0.75

Table 2
Definition of parameters and their values used for zooplankton groups

Definition	Mesozoo	Microzoo
Maximum zooplankton grazing rate (d^{-1})	g_l=1.2	g_s=2.0
Zooplankton mortality rate (d^{-1})	λ_l=0.04	λ_s=0.04
Zooplankton excretion rate (d^{-1})	μ_l=0.07	μ_s=0.07
Assimilation efficiencies	δ_l=0.75	δ_s=0.75
Half saturation constant for zooplankton grazing (mmol N m^{-3})	K_l=0.7	K_s=0.7
Q_{10} parameter for temperature limitation	Q_d=2.0	Q_d=2.0

3. Results and discussion

The strategy adopted here to study the Black Sea *E. huxleyi* bloom dynamics is to first describe in detail a typical observed situation, the so-called the "Control Run" simulation, which reproduces major observed features of the annual plankton and nutrient cycles using the optimum parameters list provided in Tables 1–3. The next step is to examine most critical processes in the development of summer coccolithophore blooms by assigning different values for some parameters.

3.1. Annual plankton cycles and community structure: the "Control Run"

The annual distributions of nutrients (phosphate, nitrate, and ammonium) in the water column (Fig. 3) show an intrusion into the euphotic layer in winter months due to strong wind and a buoyancy (cooling)-induced convective overturning (see Oguz et al., 1999

for details of the winter mixing process). Nutrients, in fact, start building up in gradually deepening mixed layer by the beginning of the cold season in November. By mid-February, phosphate and nitrate concentrations within approximately 50 m deep winter surface mixed layer reach 0.25 and 2.5 μM, respectively. Ammonium concentration, on the other hand, remains at its background level of about 0.05 μM, implying that biological production and subsequent remineralization–nitrification cycle are not yet effective in the ecosystem during this biologically inactive phase of the annual cycle due to strong temperature and light limitations. By the beginning of March cooling stops gradually, and the mixed layer becomes warmer and shallower. The sharp changes in temperature and vertical mixing during this period have already been shown in Fig. 6 of Oguz et al. (1999). Penetration of more photosynthetically available radiation into the deeper levels of the water column during this period is evident by the light limitation function (Fig. 4).
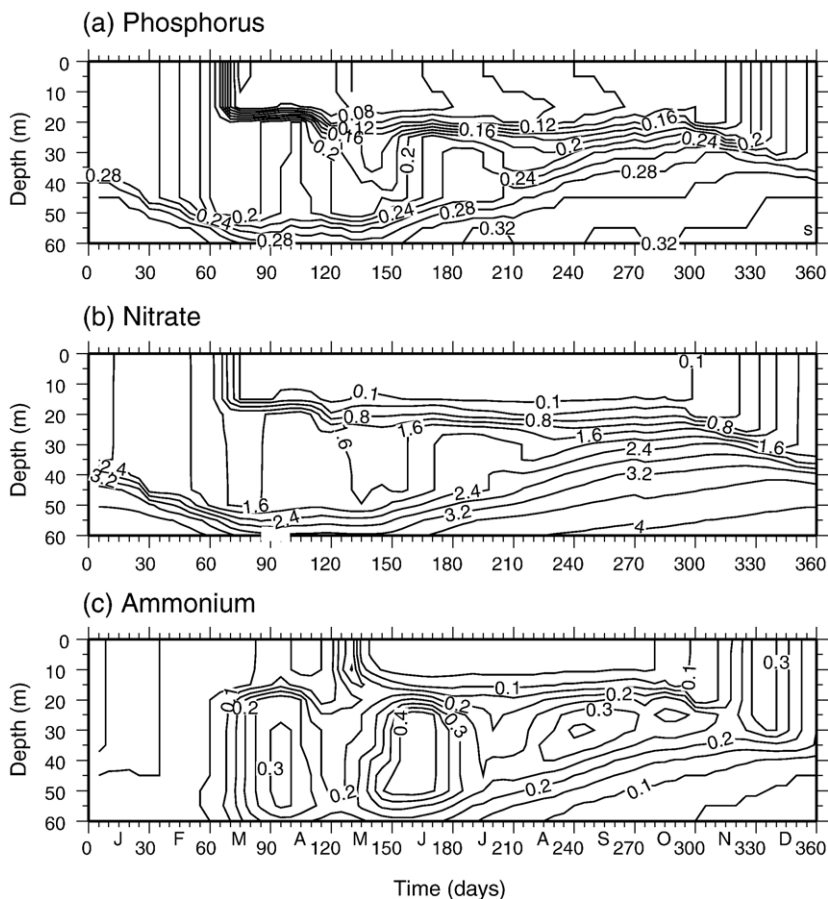

Fig. 3. The model derived annual distributions of (a) phosphate, (b) nitrate and (c) ammonium concentrations (in μM) in the upper part of water column during the perpetual year of the Control Run. The contour interval is 0.02 μM for phosphate, 0.4 μM for nitrate and 0.05 μM for ammonium.
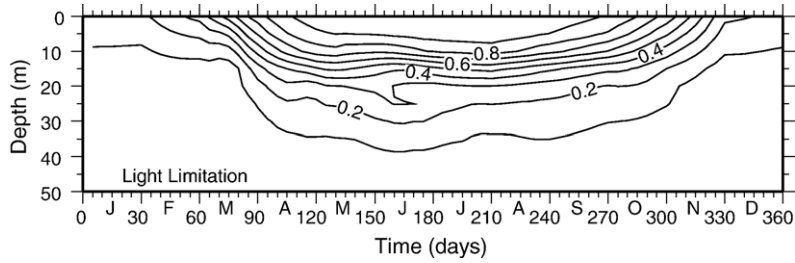
Fig. 4. Annual distribution of the light limitation function computed by Eq. (6) using the value of 0.1 for slope of the *PI* curve.

Both phosphate and nitrate concentrations undergo sharp reductions within the upper 20 m layer in the subsequent ~10 days. This period corresponds to the classical strong new production-based diatom bloom (Fig. 5a), which is preferentially confined to the upper 20 m layer reflecting strong light limitation fur-
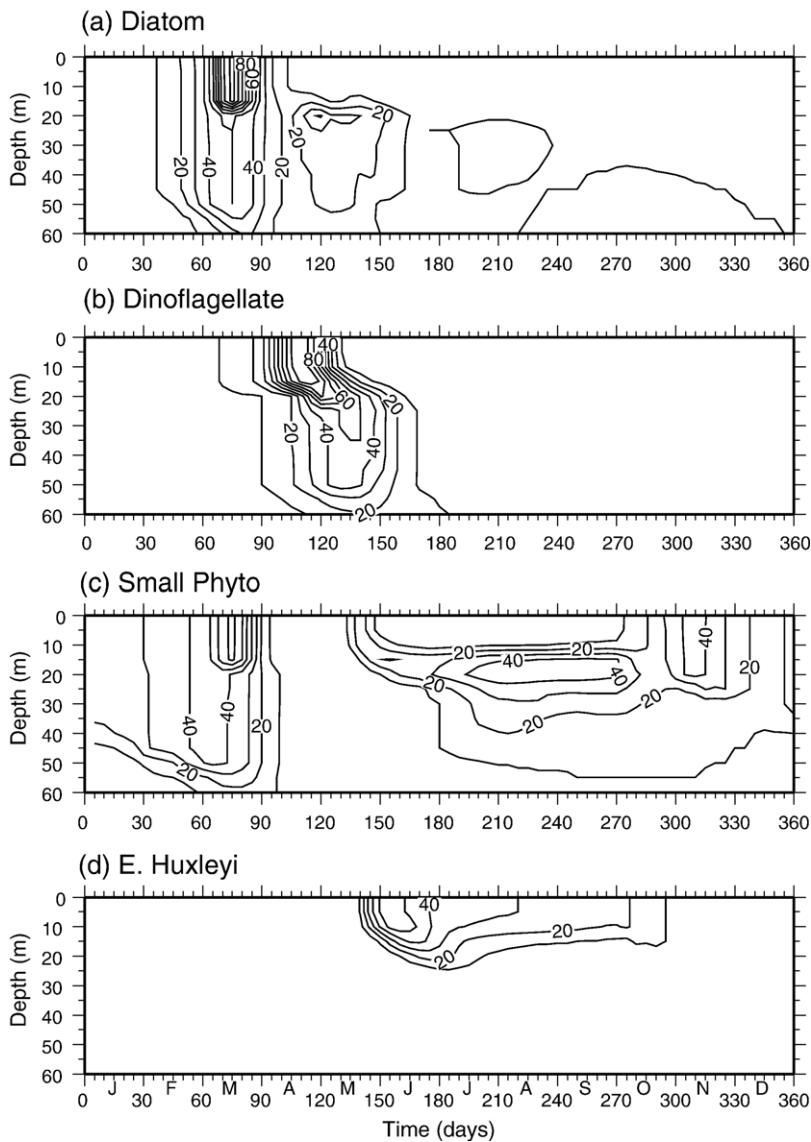

Fig. 5. The model derived annual distributions of (a) diatom, (b) dinoflagellate, (c) small phytoplankton, and (d) *E. huxleyi* biomass (mg C m^{-3}) during the perpetual year of the control run. The contour interval is 10 mg C m^{-3} for all plots.

ther below (Fig. 4). The bloom however extends partially up to the base of the euphotic zone, around 50 m at the initial phase of the bloom when the deep convective overturning mechanism is still active. The diatom biomass within the surface mixed layer reaches 100 mg C m^{-3} (assuming 1 mmol N equals to $12*6.625$ mg C) while the biomass in subsurface levels is around 30 mg C m^{-3}.

The maximum phytoplankton growth rates provided in Table 1 apply for temperature at 20 °C and higher. They are therefore expected to reduce to a certain extent during the colder autumn and spring months in the surface mixed layer as well as within the cold intermediate layer (the remnant of the convectively formed winter mixed layer with $T < 8$ °C in summer months. According to the Q_{10} formulation used, the maximum diatom growth rate of 2.9 d^{-1} was reduced by about 40% to 1.7 d^{-1} during the early March at colder water temperatures. As one of the fastest growing phytoplankton groups in the model with the temperature-controlled maximum growth rate of about 0.9 d^{-1}, picophytoplankton group also contributes to the March bloom event with the maximum biomass of 60 mg C m^{-3} (Fig. 5c). Picophytoplankton group outcompetes coccolithophores since the latter group has more strongly limited by solar radiation during this particular period of the year.

The majority of nutrients residing below the layer of surface-intensified diatom bloom were generally unused due to lack of sufficient photosynthetically available radiation during the early spring period (Fig. 4). Those used are recycled back following the biological pump as indicated by gradual increase of subsurface ammonium and nitrate concentrations up to ~0.3 and ~1.8 μM, respectively, during March–April (Fig. 3c). On the other hand, both phosphate and nitrate concentrations recycled within the surface mixed layer following the completion of diatom bloom are immediately consumed by the dinoflagellate community. Being diatoms and small phytoplankton community subject to zooplankton grazing and coccolithophore growth still subject to strong light limitation, dinoflagellates with temperature-controlled maximum growth rate of about 0.6 day^{-1} attain maximum biomass of 90 mg C m^{-3} within the mixed layer during the first half of April (Fig. 5b). In May, the core of the dinoflagellate bloom shifts below the seasonal thermocline, where more nutrients are available and light conditions are now more tolerant for their growth as compared to the previous month (Fig. 4). By the end of May, the subsurface dinoflagellate bloom is replaced by gradually increasing picophytoplankton production. Their bio-

mass reaches ~40 mg C m^{-3} below the thermocline at depths of 20–30 m in August and September (Fig. 5c). Further below, the strong light limitation prevents any phytoplankton activity. The small phytoplankton group also dominates the autumn community within the surface mixed layer in November, which then declines in December when the light limitation imposes, once again, a strong constraint on their growth.

The *E. huxleyi* population starts growing immediately after depletion of the dinoflagellate bloom in the surface mixed layer (Fig. 5d) by using the ammonium resources made available after the dinoflagellate bloom. Confined within the upper 20 m layer of most favorable light and temperature conditions for their growth, it reaches its highest intensity in the second half of May–early June (50 mg C m^{-3}), then declines gradually in July and August. Because *E. huxleyi* bloom occurs at water temperatures greater than 20 °C, temperature limitation of its maximum growth rate is insignificant during the blooms (Fig. 4). The phosphorus limitation function is greater than 0.9 as compared to the nitrogen limitation function of around 0.2 during *E. huxleyi* growth in May–August (not shown). The nitrogen limitation thus imposes more severe constraint for the growth of *E. huxleyi* population in the Black Sea.

3.2. Comparison with observations

A partial support for the species succession predicted by the model is provided by six set of observations performed during March 1998, April 1995, May–June 2001, July 1996, September 1998, October 1995 within interior waters of the southern Black Sea (Eker-Develi and Kideys, 2003) as well as May–July 1992 measurements performed within the northern sector of the Black Sea (Mankovsky et al., 1996). Diatoms were found to contribute to 97% of total phytoplankton biomass during March 1998 observations, whereas dinoflagellates constituted its 83% during April 1995. The May–July 1992 sampling indicated dense coccolithophore blooms up to 6 million cells per liter during the late-May and early-June with decreasing cell counts towards July. The lack of coccolithophore bloom inferred by the satellite data during May–June 2001 (Cokacar, 2005) was also supported by in situ measurements suggesting dinoflagellate-dominated system. A similar sequence of phytoplankton species succession during the spring and summer months has been reported for the western coastal waters (Moncheva and Krastev, 1997). Contrary to the domination of small phytoplankton in the

model simulations, the observed phytoplankton species composition during the summer and autumn months is mainly formed by the combination of dinoflagellates and diatoms with some additional contributions from *E. huxleyi* and flagellates.

Assuming the C:Chl ratio of 50, and C:N ratio of 12*6.625 mg C/mmol N, the sum of diatom, dinoflagellate and picophytoplankton annual biomass distribution (expressed in terms of chlorophyll concentration) in Fig. 6a resembles very closely the observed monthly composite chlorophyll distribution shown in Fig. 6b from Vedernikov and Demidov (1997). Concentrations of more than 2 mg m^{-3} distributed uniformly over 40–50 m thick euphotic zone during the late winter–early spring period, ~1.0 mg m^{-3} within the surface mixed layer of 25–30 m during autumn months, and

0.3–1.0 mg m^{-3} below the seasonal thermocline during summer months are reproduced satisfactorily by the model.

Fig. 6a also includes *E. huxleyi* biomass distribution (in chlorophyll units as well), where the timing of most dense biomass agrees well with the observations (see Fig. 1) obtained by the analysis of six year-long (1997–2002) satellite data. Because of low chlorophyll content of *E. huxleyi* cells, contrary to the case of diatoms and dinoflagellates, the summer *E. huxleyi* bloom signature can not however be traced in Fig. 6b. An indirect support for the *E. huxleyi* biomass distribution may be provided by comparing the computed and observed coccolith concentrations. The model estimate of 150 mg C m^{-3} total (the sum of attached and detached) coccolith concentrations (Fig. 7) lies within 100-to-200
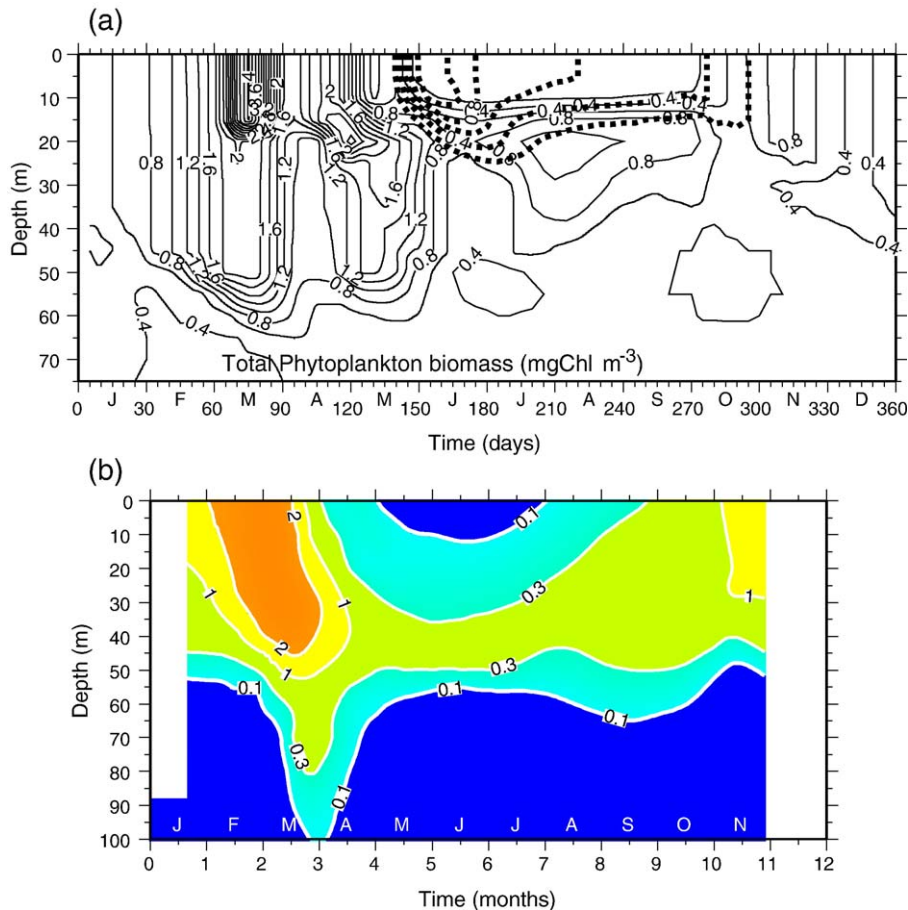

Fig. 6. (a) The annual distributions of (a) the sum of model computed diatom, dinoflagellate and small phytoplankton (continuous lines) and of *E. huxleyi* (broken lines) expressed in terms of chlorophyll concentration (mg Chl m^{-3}) with the contour interval is 0.2, and (b) monthly variations of observed chlorophyll concentration distribution (mg m^{-3}) within the upper 100 m of the water column for the interior basin of the Black Sea. It is reproduced from Fig. 5 of Vedernikov and Demidov (1997), and based on the monthly averaged data from 16 cruises performed during the 1978–1992 period.
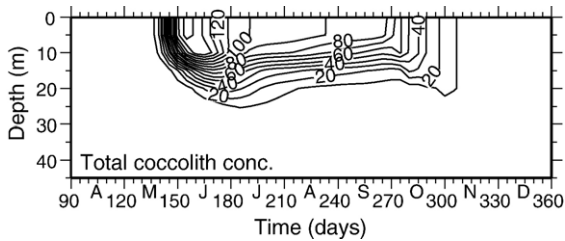
Fig. 7. Annual distributions of the total (the sum of attached and detached) coccolith concentrations (mg C m^{-3}). The contour interval is 20 mg C m^{-3}.

mg C m^{-3} range estimated by the satellite data in our companion paper by Cokacar et al. (2004). The maximum *E. huxleyi* biomass values of about 50–60 mg C m^{-3} computed in our simulations therefore seem to be reasonable.

3.3. Critical processes controlling E. huxleyi growth

Numerous field studies, especially in different parts of the North Atlantic Ocean, showed bloom occurrence of *E. huxleyi* in highly stratified and nutrient depleted waters within shallow mixed layer of ~30 m or less in the early summer following the decline of the spring bloom event (e.g., Head et al., 1998; Iglesias-Rodriguez et al., 2002). This is also the case observed in the Black Sea, and our model simulations presented in the previous section support all these observational findings. In addition to the stratification, some other factors such as photoinhibition, zooplankton selective grazing, N : P ratio, extra light shading due to coccoliths were suggested as potentially important processes governing *E. huxleyi* bloom formation and intensity (Paasche, 2002; Merico et al., 2004).

In general, photoinhibition of other phytoplankton groups at irradiance values greater than ~200 W m^{-2} was generally found to promote *E. huxleyi* bloom development in surface waters. The higher light saturation level of *E. huxleyi* with respect to diatoms and dinoflagellates make them more competitive at higher light intensities when the others are photoinhibited. *E. huxleyi* bloom development in the Black Sea takes place at radiance values of about 150 W m^{-2}, and thus photoinhibition of other algae groups is not a particularly effective process. On the other hand, the way in which irradiance increases during the *E. huxleyi* growth period appears to be critical for the bloom characteristics. In the "Control Run", the slope of the *PI* curve for *E. huxleyi* group was specified as the half of the value assigned for other groups (i.e. $a_e = 0.005$ m^2 W^{-1}), implying the half saturation light level of 100 W

m^{-2}. This value is a typical choice suggested by observations (Nanninga and Tyrrell, 1996; Paasche, 2002), and indicates higher light requirement for *E. huxleyi* growth with respect to other algae groups. It is actually one of the primary reasons why *E. huxleyi* blooms take place sometime after the spring bloom formation of other algae groups. It also explains why the picophytoplankton group having more or less similar maximum growth rate value but with higher initial slope of the *PI* curve is able to grow synchronously with *E. huxleyi* at deeper levels with lower light intensities. A further implication is possibility of earlier *E. huxleyi* bloom development under warmer and clear sky conditions in spring months. This is confirmed by repeating the "Control Run" with the slope of the *PI* curve to be identical for all phytoplankton groups at the value of 0.01 m^2 W^{-1} (i.e., the half saturation light value of ~50 W m^{-2}). The resulting annual phytoplankton structure in the water column (Fig. 8a) possesses earlier initiation of the *E. huxleyi* growth in mid-April, and attaining slightly higher maximum biomass value in May.

The shading effect of coccoliths, generated as a by-product of *E. huxleyi* blooms, to the light penetration in the water column is incorporated into the model (see Eq. (7) in Appendix). As shown in Fig. 5c, coccoliths limit production of small phytoplankton group to the upper 20 m during the most intense period of *E. huxleyi* bloom event by reducing light penetration. Picophytoplankton group can start growing at deeper part of the euphotic zone only during the declining phase of *E. huxleyi* bloom. In addition, as for the limitation introduced by the slope of the *PI* curve, the presence of dense coccolith concentration hinders deeper penetration of *E. huxleyi* community development during later stage of the bloom.

In the Control Run, nitrate half saturation constants of phytoplankton groups were specified proportional to their maximum growth rates with the highest value for diatoms (0.5 μM) and lowest for dinoflagellates (0.23 μM). The choice of the value of 0.38 μM for *E. huxleyi* provides a slight competitive advantage against picophytoplankton having the value of 0.3 μM. Additional simulations using two extreme values of the *E. huxleyi* nitrate half saturation constants of $K_{ne} = 0.2$ and 0.5 μM yield very similar biomass distributions of *E. huxleyi* compared to that given by the "Control Run" (Fig. 8b). The choice of nitrate half saturation constant therefore appears to be not so critical for the *E. huxleyi* growth in the Black Sea, as long as it is not exceptionally greater than those of the other groups. Whatever is the choice of K_{ne}, it will

promote a bloom structure during the early summer, because the other groups have already flourished and have been subject to the mortality and stronger zoo-

plankton grazing pressure; thus, they will no longer be able to compete with *E. huxleyi*.

Zooplankton grazing rates and food preferences are generally most sensitive parameters in marine ecosystem models, especially in highly productive regions and seasons. The food preference rates are often poorly known. Their specifications involve great deal of uncertainty, and are subject to some tuning for obtaining realistic model simulations compatible with observations. The "Control Run" simulation considers the most dominant microzooplankton grazing on *E. huxleyi* by choosing the food preference coefficient $b_{se} = 0.6$ as compared to $b_{ss} = 0.2$ for the picophytoplankton group. Changing the original food preference coefficient of $b_{se} = 0.6$ to a higher value of 0.8 reduces the *E. huxleyi* biomass only slightly. Reducing the food preference coefficient to 0.4, on the other hand, weakens their grazing, and therefore gives rise to slightly stronger growth of *E. huxleyi* population during the entire summer period (Fig. 8c).

Changing the food preference value of microzooplankton on picophytoplankton group can also alter *E. huxleyi* biomass indirectly. For example, increasing it from $b_{ss} = 0.2$ to 0.4 doubles the grazing pressure and leads to depletion of picophytoplankton stocks, and a compensatory increase in *E. huxleyi* biomass (Fig. 8d).

The impact of mesozooplankton grazing on *E. huxleyi* is more severe since their growth occurs during the period of high mesozooplankton biomass right after the intense spring bloom phase. The "Control Run" considers weak mesozooplankton grazing of *E. huxleyi* specified by $b_{le} = 0.05$. In the case of stronger grazing, represented by $b_{le} = 0.15$, availability of high mesozooplankton biomass in the system during the early summer period introduces an appreciable impact on grazing which ultimately results in considerable reduction in *E. huxleyi* biomass (Fig. 8e). Its further increase to $b_{le} = 0.25$ causes complete depletion of *E. huxleyi* in the ecosystem, suggesting consumption of the entire *E. huxleyi* stock by mesozooplankton. This process is accompanied with more effective growth of picophytoplankton community in the surface mixed layer.
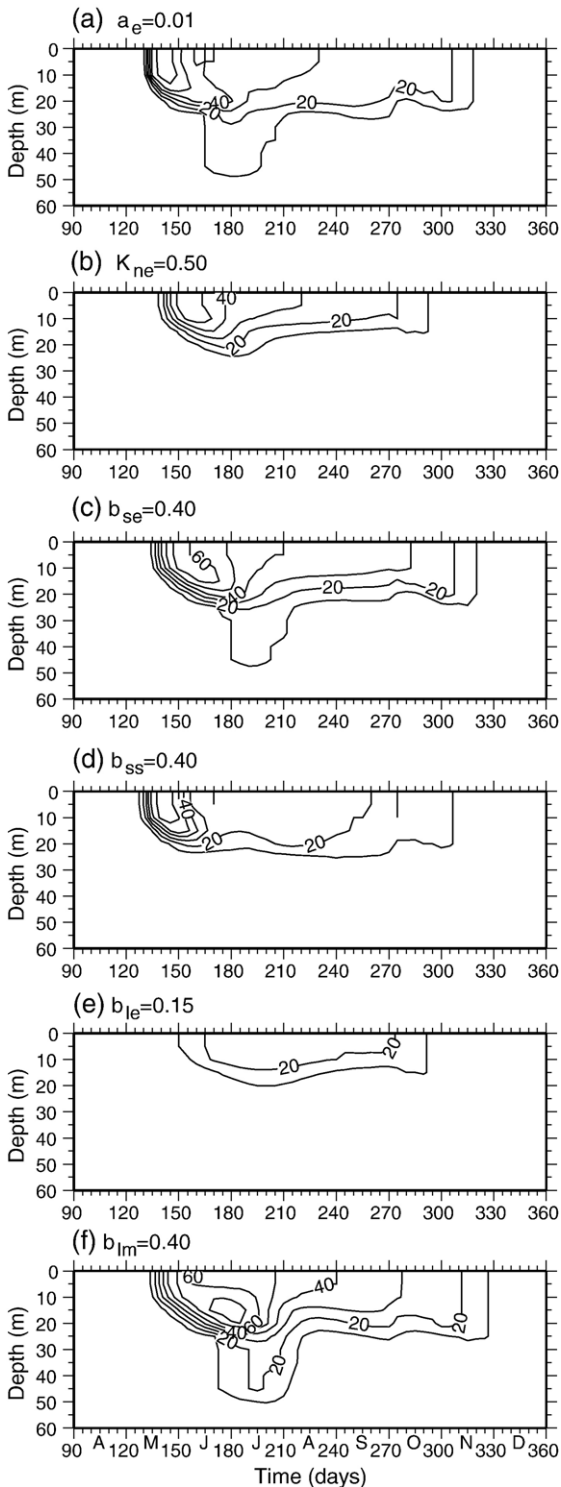
Fig. 8. The annual distribution of *E. huxleyi* biomass (mg C m^{-3}) computed by changing the value of (a) the slope of the *PI* curve from 0.005 to 0.01 m^2 W^{-1}, (b) the nitrate half saturation constant from 0.2 to 0.5 μM, (c) the microzooplankton food preference coefficient on *E. huxleyi* from 0.6 to 0.4, (d) the microzooplankton food preference coefficient on small phytoplankton group from 0.2 to 0.4, (e) the mesozooplankton food preference coefficient on *E. huxleyi* from 0.05 to 0.15, (f) the mesozooplankton food preference coefficient on microzooplankton from 0.2 to 0.4. The contour interval is 10 mg C m^{-3}.

The impact of zooplankton grazing on the food web is in fact quite nonlinear. For example, increasing the mesozooplankton food preference on microzooplankton from 0.2 to 0.4, leads to an appreciable reduction on microzooplankton biomass during the spring–early summer period, which indirectly releases some of the grazing pressure of microzooplankton on *E. huxleyi* and give rise to their higher biomass during the summer–autumn (Fig. 8f).

The last group of sensitivity experiments explores whether or not phosphate limitation can be effective for controlling *E. huxleyi* growth in the Black Sea. To this end, the phosphorus to nitrogen ratio of 1/10 specified in the Control Run is replaced by 1/22, and the total phosphorus concentration in the water column is reduced by one half as well. Even under this setting, which is prone to a strong phosphorus limitation, nitrogen limitation was found to still effectively control *E. huxleyi* growth with a similar biomass distribution depicted in Fig. 5d.

4. Conclusions

A process-oriented model provided a quantitative support for the satellite-based interpretation of the early summer *E. huxleyi* blooms in the Black Sea, and explored its growth characteristic and variability in terms of intensity, duration and timing. In accord with the observations, the simulations showed flourishing of the *E. huxleyi* population right after dense populations of diatoms in March and dinoflagellates in April. In May, both *E. huxleyi* and picophytoplankton population started increasing within the mixed layer by using regenerated nutrients available within the near-surface waters under moderate light conditions. Picophytoplankton population later dominated within the subsurface layer whereas *E. huxleyi* community remained to confine within the surface mixed layer. Hence, the Black Sea ecosystem is able to regularly maintain a moderate level *E. huxleyi* bloom development as a part of its seasonal phytoplankton succession. The bloom intensity is however approximately 5-fold smaller than those measured in the North Atlantic (Tyrrell and Taylor, 1996) and the Bering Sea shelf (Merico et al., 2004), because of relatively more oligotrophic character of the Black Sea interior basin.

The observed sequence of diatom–dinoflagellate–*E. huxleyi*–picophytoplankton bloom events taking place during the spring–early summer period arises as a response to their different maximal growth rates with highest for diatoms and lowest for dinoflagellates. *E. huxleyi* and picophytoplankton have comparable inter-mediate rates with a growth advantage of the latter group at lower light levels. The diatom and picophytoplankton groups, having two highest net growth rate characteristics, flourish first in March. Once their bloom tends to decline mainly because of their grazing by zooplankton, dinoflagellates start flourishing intensively in April. The light intensity still limits *E. huxleyi* growth during this period, but diatoms continue to contribute to the overall phytoplankton population. Towards the end of April, the surface mixed layer experiences simultaneous growth of *E. huxleyi* and picophytoplankton, the latter of which later confine preferentially into the subsurface layer of the euphotic zone. Because of their strong light requirement, the growth of *E. huxleyi* population is limited to approximately upper 20 m layer. The presence of the Cold Intermediate Layer with $T < 8$ °C below the surface mixed layer is also a factor that limits their subsurface growth. In general, their success in blooming against small phytoplankton group is not much affected by some small changes in the growth parameters suggesting that they can grow in fairly wide range of environmental conditions. Though implemented specifically to the Black Sea in the present application, the model serves a basic tool to investigate the fate of CO_2 in the water column when integrated with the carbonate chemistry. This is one of the limitations of the present global ocean carbon cycle models (e.g. Moore et al., 2002).

Appendix A. Governing equations

The local temporal variation of any state variable F is expressed by an equation of the form

$$\frac{\partial F}{\partial t} + \frac{\partial (w_b F)}{\partial z} = \frac{\partial}{\partial z}\left[K\frac{\partial F}{\partial z}\right] + \Re(F) \tag{1}$$

where t is time, z is the vertical coordinate, ∂ denotes partial differentiation, K is the vertical turbulent diffusion coefficient. w_b represents the sinking velocity for diatoms and detrital material, and is set to zero for the other compartments. $\Re(F)$ denotes source and sink terms whose explicit forms are given below.

A.1. Phytoplankton module

The source-sink terms for all phytoplankton groups are expressed by

$$\Re(P_k) = \Phi_k P_k - [G_s(P_k)Z_s + G_l(P_k)Z_l] - \lambda_k P_k \qquad (2)$$

where the subscript k denotes either d for diatoms, f for dinoflagellates, e for *E. huxleyi* and s for small phytoplankton. Accordingly, temporal changes in phytoplankton standing stocks are controlled by primary production (the first term), zooplankton grazing losses (the terms within the square brackets) and physiological mortality (the last term). The growth rate Φ_k that limits the primary production is defined by

$$\Phi_k = g_k \alpha_k(I) f_k(T) \cdot \min[\beta_{t,k}(N_n, N_a), \beta_{p,k}(N_p)] \qquad (3)$$

where g_k, denotes maximum specific growth rate at 20 °C, $\alpha_k(I)_k$, the limitation function due to light, $f_k(T)$ the limitation function due to temperature. The last term represents the nutrient uptake expressed as the minimum of total nitrogen (sum of nitrate and ammonium) limitation $\beta_{t,k}(N_n, N_a)$ and phosphorus limitation $\beta_{p,k}(N_p)$. Following Liebig's law of the minimum, the nutrient uptake rate is thus limited by either inorganic nitrogen or phosphorus. The total nitrogen limitation function is specified by the sum of nitrate and ammonium limitations expressed, respectively, according to the Monod kinetics in the forms

$$\beta_{n,k}(N_n) = [N_n/(K_{n,k} + N_n)]\exp(-\varphi N_a) \qquad (4a)$$

$$\beta_{a,k}(N_a) = N_a/(K_{a,k} + N) \qquad (4b)$$

where $K_{n,k}$ and $K_{a,k}$ represent half saturation constants for nitrate and ammonium limitations respectively. Similarly, the phosphorus limitation function is given by

$$\beta_{p,k}(N_p) = N_p/(K_{p,k} + N_p) \qquad (5)$$

Light limitation for all phytoplankton groups is represented by the tangent hyperbolic function

$$\alpha_k(I) = \tanh[a_k I(z,t)] \qquad (6)$$

where the constant parameter a_k quantifies the slope of P–I curve. The photosynthetically available solar radiation $I(z,t)$ decays exponentially with depth from its surface value I_s according to the extinction parameter k defined by

$$k = k_w + k_p \int_0^z (P_d + P_f + P_e + P_s)\,dz$$
$$+ k_c \int_0^z (C_a^* + C_f^* + D_n)\,dz \qquad (7)$$

where k_w denotes the clear water contribution, and k_p, k_c represent the self-shading coefficients due to turbid water contributions of living and non-living constituents, respectively In Eq. (7), C_a^* and C_f^* denote concentrations of attached and free coccoliths which are converted from carbon to nitrogen unit in order to be compatible with the detritus concentration D_n expressed in nitrogen units within the second integral of Eq. (7).

The temperature limitation function is given by

$$f_k(T) = Q_{10,k}^{(T-20)/10} \qquad (8)$$

where Q_{10} value for all phytoplankton groups is taken as 1.5. The temperature T is provided at each time step by the physical model. A similar expression is also used for zooplankton with a Q_{10} value of 2.0.

A.2. Zooplankton module

The microzooplankton and mesozooplankton biomass are controlled by ingestion (which is assimilated part of the grazing), predation as well as mortality and excretion. They are expressed by

$$\Re(Z_s) = \gamma_s \left[\sum_k G_s(P_k) + G_l(D_n) \right] Z_s$$
$$- G_l(Z_s)Z_l - \mu_s Z_s - \lambda_s Z_s \qquad (9)$$

$$\Re(Z_l) = \gamma_l \left[\sum_k G_l(P_k) + G_l(D_n) + G_l(Z_s) \right]$$
$$\times Z_l - \mu_l Z_l - \lambda_l Z_l. \qquad (10)$$

In Eqs. (9) and (10), the first terms within the first square brackets describe ingestion of phytoplankton by microzooplankton and mesozooplankton, respectively. The second terms signify detritus consumption by the zooplankton groups. The last term within the square bracket of Eq. (10) represents ingestion of microzooplankton by mesozooplankton with a similar term of the opposite sign in Eq. (9). The last two terms describe excretion and mortality, respectively, which are both expressed in the linear form. As shown by Oguz et al. (1999), the choice of linear mortality, when compared to its quadratic form, does not introduce oscillations resulting from prey–predator interactions.

Grazing/predation terms for microzooplankton and mesozooplankton in Eqs. (9), (10) are represented in the Michaelis–Menten functional form in terms of the max-

imum rate g_k, the temperature limitation function $f_k(T)$, and food capture efficiency coefficients $b_{k,i}$ by

$$G_k(P_i) = g_k f_k(T) \frac{b_{k,i} \cdot P_i}{K_k + \sum_i b_{k,i} \cdot P_i} \qquad (11)$$

where the subscript k denote either s for the microzooplankton group or l for the mesozooplankton group. The subscript i runs over the four phytoplankton groups. $b_{k,i}$ denotes the constant coefficient of food preference for kth predator on ith prey. Each of these coefficients vary between zero (no preference) and one (maximum preference).

A.3. Formulation of nitrogen and phosphorus cycles

The source-sink terms for the detrital organic nitrogen and phosphorus are expressed, respectively, by

$$\begin{aligned}\Re(D_n) &= [\text{DETR}] - \varepsilon_n D_n \\ \Re(D_p) &= r_{PN}[\text{DETR}] - \varepsilon_p D_p \end{aligned} \qquad (12a,b)$$

where r_{PN} denotes a constant phosphorus to nitrogen ratio, ε_n and ε_p are the remineralization rates for detrital nitrogen and phosphorus, respectively. A separate equation for D_p is introduced in Eq. (12b) in order to be able to specify a different remineralization rate for detrital phosphorus as compared to that of detrital nitrogen. DETR is given by

$$\begin{aligned}\text{DETR} &= (1 - \gamma_l)\left[\sum_k G_l(P_k) + G_l(Z_s)\right]Z_l \\ &+ (1 - \gamma_s)\left[\sum_k G_s(P_k)\right]Z_s \\ &+ \left[\sum_k \lambda_k P_k + \lambda_s Z_s + \lambda_l Z_l\right] \\ &- \left[\gamma_l G_l(D_n)Z_l + \gamma_s G_s(D_n)Z_s\right] \end{aligned} \qquad (13)$$

which represents the group of terms describing unassimilated (i.e. egested) parts of the food grazed by zooplankton (the first and second square brackets), phytoplankton and zooplankton mortalities (the third square bracket), and consumption of detritus by zooplankton groups (the last square bracket).

The change in ammonium concentration is governed by the losses due to its uptake in the primary production and nitrification, and the sources due to excretion by zooplankton and remineralization. They are expressed by

$$\begin{aligned}\Re(N_a) = &-\sum_k \left(\frac{\beta_{a,k}}{\beta_{t,k}}\right)\Phi_k P_k - \Omega_a N_a + \varepsilon_n D_n \\ &+ \mu_s Z_s + \mu_l Z_l \end{aligned} \qquad (14)$$

The change in nitrate stocks is controlled by the difference between nitrate uptake and nitrification, as expressed by

$$\Re(N_n) = -\sum_k \left(\frac{\beta_{n,k}}{\beta_{t,k}}\right)\Phi_k P_k + \Omega_a N_a \qquad (15)$$

Similarly, the source-sink terms for dissolved inorganic phosphate are

$$\Re(N_p) = -r_{PN}\sum_k \Phi_k P_k + \varepsilon_p D_p + r_{PN}[\mu_s Z_s + \mu_l Z_l] \qquad (16)$$

A.4. Formulation for the attachment end detachment of coccoliths

Following Tyrrell and Taylor (1996) attached and detached coccolith concentrations (in mg calcite C m^{-3}) generated as byproducts of *E. huxleyi* blooms are computed by

$$\begin{aligned}\Re(C_a) = &C_{max}\alpha_k(I)f_k(T)r_{CN}P_e \\ &- [G_s(C_a)Z_s + G_l(C_a)Z_l] - \lambda_e C_a - \Gamma \end{aligned} \qquad (17)$$

$$\Re(C_d) = \Gamma + \lambda_e C_a - [G_s(C_d)Z_s + G_l(C_d)Z_l] - \Theta C_d \qquad (18)$$

where the detachment rate Γ is represented by

$$\Gamma = \max[\Gamma_d(C_a - \Pi_{max}r_{CN}P_e), \Gamma_{dmin}C_a] \qquad (19)$$

The first term in Eq. (17) denotes the calcification rate of whole *E. huxleyi* cells in which the maximum rate $C_{max}r_{CN}P_e$ is limited by the light and temperature dependence. r_{CN} is the carbon to nitrogen ratio to convert P_e from nitrogen to carbon unit and taken as $12 * 6.625$ mg organic C/mmol N. The terms within the square brackets represent the losses of attached coccoliths during the grazing of *E. huxleyi* cells by zooplankton community. Similarly, the third term is the loss due to mortality of cells, and the last term is the detachment rate. In Eq. (18), the loss due to mortality of cells and detachment rate enter as the source terms to the temporal rate of change of detached coccolith concentrations. Detached coccoliths are lost during the consumption of *E. huxleyi* by zooplankton community, and dissolution of calcite of detached coccoliths. Eq. (19) suggests that the detachment rate is computed by the excess of attached coccolith concentration over the maximum coccolith concentration allowed per *E. huxleyi* cell (i.e. the first term in the square bracket). If there is no excess coccolith concentration, then detach-

ment occurs at a negligible rate given by the second term in the square bracket of Eq. (19).

References

Aknes, D.L., Egge, J.H., Rosland, R., Heimdal, B., 1994. Representation of *Emiliania huxleyi* in phytoplankton simulation models. A first approach. Sarsia 79, 291–300.

Benli, H.A., 1987. Investigation of phytoplankton distribution in the southern Black Sea and its effect on particle flux. In: Degens, E.T., Izdar, E. (Eds.), Particle Flux in the Ocean, Mitteilungen des Geologisch-Palaontologischen Institutes, vol. 62. Universitat Hamburg, pp. 77–87.

Cokacar, T., 2005. Atmospheric correction of ocean color for the mineral dust aerosol over the Mediterranean Sea and remotely sensed characterization of coccolithophore blooms in the Black Sea. Ph.D Thesis, Middle East Technical University, Institute of Marine Sciences. 139 pp.

Cokacar, T., Kubilay, N., Oguz, T., 2001. Structure of *Emiliania huxleyi* blooms in the Black Sea surface waters as detected by SeaWIFS imagery. Geophys. Res. Lett. 28 (24), 4607–4610.

Cokacar, T., Oguz, T., Kubilay, N., 2004. Interannual variability of the early summer coccolithophore blooms in the Black Sea: impacts of anthropogenic and climatic factors. Deep-Sea Res. I 51, 1017–1031.

Egge, J.K., Heimdal, B.R., 1994. Blooms of phytoplankton including *Emiliania huxleyi* (Haptophyta). Effects of nutrient supply in different N:P ratios. Sarsia 79, 333–348.

Eker, E., Georgieva, L., Senichkina, L., Kideys, A.E., 1999. Phytoplankton distribution in the western and eastern Black Sea in spring and autumn 1995. ICES J. Mar. Sci. 56, 15–22 (Supplement).

Eker-Develi, E., Kideys, A.E., 2003. Distribution of phytoplankton in the southern Black Sea in summer 1996, spring and autumn 1998. J. Mar. Syst. 39, 203–211.

Gregoire, M., Beckers, J.M., Nihoul, J.C.J., Stanev, E., 1998. Reconnaissance of the control Black Sea's ecohydrodynamics by means of a 3D interdisciplinary model. J. Mar. Syst. 16, 85–106.

Gregoire, M., Soetaert, K., Nezlin, N., Kostianoy, A., 2004. Modelling the nitrogen cycling and plankton productivity in the Black Sea using three dimensional interdisciplinary model. J. Geophys. Res. 109, C05007. doi:10.1029/1001JC001014.

Hay, B.J., Honjo, S., 1989. Particle sources in the present and Holocene Black Sea. Oceanography 2, 26–31.

Head, R.N., et al., 1998. The hydrography and biology of a bloom of the coccolithophorid *Emiliania huxleyi* in the northern North Sea. J. Sea Res. 39, 255–266.

Hulburt, E.M., 1990. Description of phytoplankton and nutrient in spring in the western North Atlantic Ocean. J. Plankton Res. 12, 1–28.

Iglesias-Rodriguez, M.D., et al., 2002. Representing key phytoplankton functional groups in ocean carbon cycle models: coccolithophorids. Global Biogeochem. Cycles 16, 1100. doi:10.1029/2001GB001454.

Karl, D.M., Knauer, G.A., 1991. Microbial production and particle flux in the upper 350 m of the Black Sea. Deep-Sea Res. 38 (Supp. 2A), S655–S661.

Kubilay, N., Kocak, M., Cokacar, T., Oguz, T., Kouvarakis, G., Mihalopoulos, N., 2002. The influence of Black Sea and local biogenic activity on the seasonal variation of aerosol sulfur species in the Eastern Mediterranean atmosphere. Global Biogeochem. Cycles 16, 1079. doi:10.1029/2002GB001880.

Kuypers, M.M.M., et al., 2003. Anaerobic ammonium oxidation by anammox bacteria in the Black Sea. Nature 422, 608–611.

Lancelot, C., Staneva, J., Van Eeckhout, D., Beckers, J.M., Stanev, E., 2002. Modeling the impact of the human forcing on the ecological functioning of the northwestern Black Sea. Estuarine, Coastal Shelf Sci. 54, 473–500.

Lebedeva, L.P., Shushkina, E.A., 1994. Modelling the effect of *Mnemiopsis* on the Black Sea plankton community. Oceanology (Engl. Transl.) 34, 72–80.

Lebedeva, L.P., Vostokov, S.V., 1984. Studies of detritus formation processes in the Black Sea. Oceanology (Engl. Transl.) 24 (2), 258–263.

Mankovsky, V.I., et al., 1996. Long-term variability of the Black Sea water transparency and factors determining its strong decrease in the late 1980s and early 1990s. Technical Report. Marine Hydrophysical Institute, Sevastopol, Ukraine. 32 pp.

Merico, A., et al., 2004. Modelling phytoplankton succession on the Bering Sea shelf: role of climate influencers and trophic interactions in generating *Emiliania huxleyi* blooms 1997–2000. Deep-Sea Res. I 51, 1803–1826.

Mikaelyan, A.S., 1997. Long-term variability of phytoplankton communities in open Black Sea in relation to environmental changes. In: Ozsoy, E., Mikaelyan, A. (Eds.), Sensitivity to Change: Black Sea, Baltic Sea and North Sea, NATO Sci, Partnership Sub-series 2, vol. 27. Kluwer Acad, Norwell, Mass. pp. 105–116.

Moore, J.K., Doney, S.C., Kleypas, J.A., Glover, D.M., Fung, I.Y., 2002. An intermediate complexity marine ecosystem model for the global control. Deep-Sea Res. II 49, 403–462.

Moncheva, S., Krastev, A., 1997. Some aspects of phytoplankton long-term alterations off Bulgarian Black Sea Shelf. In: Ozsoy, E., Mikaelyan, A. (Eds.), Sensitivity to change: Black Sea, Baltic Sea and North Sea, NATO Sci, Partnership Sub-series 2, vol. 27. Kluwer Acad, Norwell, Mass. pp. 79–94.

Murray, J.W., Codispoti, L.A., Friederich, G.E., 1995. Oxidation–reduction environments: the suboxic zone in the Black Sea. In: Huang, C.P., O'Melia, C.R., Morgan, J.J. (Eds.), Aquatic Chemistry: Interfacial and Interspecies Precosses, ACS Advances in Chemistry Series, vol. 224, pp. 157–176.

Nanninga, H., Tyrrell, T., 1996. Importance of light for the formation of algal blooms by *Emiliania huxleyi*. Mar. Ecol., Prog. Ser. 136, 195–203.

Oguz, T., 2005. Long-term impacts of anthropogenic forcing on the Black Sea ecosystem. Oceanography 18 (2), 112–121.

Oguz, T., Ducklow, H.W., Malanotte-Rizzoli, P., Tugrul, S., Nezlin, N., Unluata, U., 1996. Simulation of annual plankton productivity cycle in the Black Sea by a one-dimensional physical–biological model. J. Geophys. Res. 101, 16585–16599.

Oguz, T., Ducklow, H.W., Malanotte-Rizzoli, P., Murray, J.W., Vedernikov, V.I., Unluata, U., 1999. A physical–biochemical model of plankton productivity and nitrogen cycling in the Black Sea. Deep-Sea Res. I. 46, 597–636.

Oguz, T., Ducklow, H.W., Malanotte-Rizzoli, P., 2000. Modeling distinct vertical biogeochemical structure of the Black Sea: dynamical coupling of the oxic, suboxic and anoxic layers. Global Biogeochem. Cycles 14, 1331–1352.

Oguz, T., Ducklow, H.W., Purcell, J.E., Malanotte-Rizzoli, P., 2001. Modeling the response of top–down control exerted by gelatinous carnivores on the Black Sea pelagic food web. J. Geophys. Res. 106, 4543–4564.

Paasche, E., 2002. A review of the coccolithophorid *Emilinia huxleyi* (Prymnesiophyceae) with particular reference to growth, coccolith

formation, and calcification–photosynthesis interactions. Phycologia 40, 503–529.

Reigman, R., Noordeloos, A.A.M., Cadee, G.C., 1992. Phaeocystis blooms and eutrophication of the continental coastal zones of the North Sea. Mar. Biol. 112, 479–484.

Sorokin, Y.I., 2002. The Black Sea Ecology and Oceanography. Backhuys Publishers, Leiden. 32 pp.

Soydemir, N., Kideys, A.E., Ekingen, G., 2003. Phytoplankton composition of the western Black Sea during the R.V Knorr cruise in May–June 2001. Second International Conference on "Oceanography of the Eastern Mediterranean and Black Sea: Similarities and Differences of Two Interconnected Basins" 14–18 October 2002, Ankara, Turkey.

Sur, H.I., Ozsoy, E., Unluata, U., 1994. Boundary current instabilities, upwelling, shelf mixing and eutrophication processes in the Black Sea. Prog. Oceanogr. 33, 249–302.

Tyrrell, T., Merico, A., 2004. *Emiliania huxleyi*: bloom observations and the conditions that induce them. In: Thierstein, H.R., Youngs, J.R. (Eds.), Coccolithophores—From Molecular Processes to Global Impact. Springer, pp. 75–97.

Tyrrell, T., Taylor, A.H., 1996. A modeling study of *Emiliania huxleyi* in the NE Atlantic. J. Mar. Syst. 9, 83–112.

Uysal, Z., et al., 1998. Phytoplankton patches formed along the southern Black Sea coast in spring and summer 1996. In: Ivanov, L.I., Oguz, T. (Eds.), Ecosystem Modeling as a Management Tool for the Black Sea, vol 1, NATO Science Series, Environmental Security, V. 47. Kluwer Academic Publishers, Netherlands, pp. 151–162.

Vedernikov, V.I., Demidov, A.B., 1997. Vertical distributions of primary production and chlorophyll during different seasons in deep part of the Black Sea. Oceanology (Engl. Transl.) 37, 376–384.